CDDpress

www.nature.com/cdd

ARTICLE OPEN

Epstein-Barr virus drives nasopharyngeal carcinoma metastasis via RNA m^{5}C modification of ICAM-1 mediated by NSUN2 and YBX3

Xiu-Zhi Wang[1,2,3,7], Jia-Xin Jiang[1,2,7], Yi-Qi Li[1,2], Yang Liu[1,2], Shuang-Yan Ye[1,2], Wei Liu[1,2], Dong-Mei Chi[1], Shuai He[1,2], Pan-Pan Wei[1,2], Hui-Qiang Huang[1], Jin-Xin Bei[1,2,4,5,6]✉ and Chun-Ling Luo[1,2]✉

© The Author(s) 2026

Epstein-Barr virus (EBV) is a critical epigenetic regulator in nasopharyngeal carcinoma (NPC) pathogenesis, primarily through well-established mechanisms involving DNA methylation and histone modifications. However, the contribution of RNA modifications, especially RNA 5-methylcytosine (m^{5}C), to EBV-driven NPC progression remains largely unclear. Here, we performed RNA bisulfite sequencing (RNA-Bis-seq) on NPC cells and observed a global elevation in RNA m^{5}C levels following EBV infection. Notably, EBV infection upregulated NSUN2, a known RNA m^{5}C methyltransferase ("writer"), through LMP1-mediated activation of the NF-κB signaling pathway, leading to RNA m^{5}C elevation. Functional assays confirmed that NSUN2 significantly enhances NPC cell migration and metastasis through its RNA m^{5}C catalytic activity. Furthermore, we identified YBX3 as a novel RNA m^{5}C-binding protein ("reader") that was simultaneously upregulated upon EBV infection. Mechanistically, NSUN2 catalyzed m^{5}C modification on ICAM-1. Subsequently, YBX3 specifically recognized the modified site, recruiting PABPC1 through interacting with its cold shock domain and thereby enhancing ICAM-1 translation. Consistently, ICAM-1 overexpression effectively rescued the metastasis defects induced by NSUN2 knockdown. Additionally, we observed significant positive correlations among NSUN2, YBX3, and ICAM-1 expression levels in NPC tissues, with their expression strongly associated with tumor progression and poor prognosis. Together, our findings reveal the crucial role of RNA m^{5}C modification in EBV-associated NPC progression, delineate the LMP1/NSUN2/YBX3/ICAM-1 signaling cascade, and suggest this regulatory axis as a potential therapeutic target for NPC.

Cell Death & Differentiation; https://doi.org/10.1038/s41418-026-01719-4

INTRODUCTION

Nasopharyngeal carcinoma (NPC) is an epithelial malignancy originating from the nasopharynx, with a particularly high prevalence in Southern China and regions of Mediterranean Africa [1, 2]. NPC pathogenesis involves a complex interplay of Epstein-Barr virus (EBV) infection, genetic predispositions, and environmental factors [3]. Each year, approximately 129,000 new NPC cases are diagnosed globally, with over 90% closely linked to EBV infection [4, 5]. Although the association between EBV and NPC has been extensively documented, highlighted by the presence of EBV-derived components within tumors and elevated plasma EBV DNA levels in NPC patients [6], the precise oncogenic mechanisms by which EBV contributes to NPC progression remain incompletely defined.

RNA 5-methylcytosine (RNA m^{5}C) is an essential post-transcriptional modification predominantly found in eukaryotic RNAs, influencing key biological processes such as mRNA stability, translation efficiency, and nuclear export [7, 8]. The m^{5}C modification is primarily catalyzed by methyltransferases of the NOL1/NOP2/sun (Nsun) family members and DNA methyltransferase 2 (DNMT2), collectively termed RNA m^{5}C "writers", while TET-family enzymes act as m^{5}C demethylases [9]. Following methylation, m^{5}C-modified transcripts are specifically recognized by RNA-binding proteins known as "readers", which subsequently mediate various downstream cellular effects [10]. Dysregulation of RNA m^{5}C modifications has been increasingly implicated in the pathogenesis and progression of multiple cancers, including lung, gastric, bladder cancers, and NPC [11–14]. For instance, in NPC, the RNA m^{5}C reader ALYREF enhances metastasis by stabilizing NOTCH1 mRNA in an m^{5}C -dependent manner[14].

Emerging evidence also highlights significant connections between EBV infection and RNA modification, particularly N(6)-methyladenosine (m^{6}A), in EBV-associated malignancies [15–17]. For example, the m^{6}A reading protein YTHDF1 suppresses EBV replication by promoting EBV RNA decay [16], and the m^{6}A demethylase FTO facilitates metastasis and invasiveness in EBV-associated gastric carcinoma (EBVaGC) via the

[1]State Key Laboratory of Oncology in South China, Guangdong Key Laboratory of Nasopharyngeal Carcinoma Diagnosis and Therapy, Guangdong Provincial Clinical Research Center for Cancer, Collaborative Innovation Center for Cancer Medicine, Sun Yat-sen University Cancer Center, Guangzhou, PR China. [2]Department of Experimental Research, Sun Yat-sen University Cancer Center, Guangzhou, PR China. [3]Shandong Blood Center, Jinan, PR China. [4]Division of Medical Oncology, National Cancer Centre, Singapore, Singapore. [5]Sun Yat-sen University Institute of Advanced Studies Hong Kong, Science Park, Hong Kong, PR China. [6]Department of Clinical Oncology, School of Clinical Medicine, Li Ka Shing Faculty of Medicine, University of Hong Kong, Hong Kong, PR China. [7]These authors contributed equally: Xiu-Zhi Wang, Jia-Xin Jiang. ✉email: beijx@sysucc.org.cn; luochl@sysucc.org.cn

Received: 5 June 2025 Revised: 14 January 2026 Accepted: 5 March 2026
Published online: 18 March 2026

m^{6}A-FOS-IGF2BP1/2 axis [18]. Recently, EBV-encoded non-coding RNA EBER1 was found to undergo m^{5}C modification, enhancing its stability and viral pathogenicity [19]. However, the broader significance and precise molecular mechanism of RNA m^{5}C modifications in EBV-driven tumorigenesis, particularly in NPC, remain unclear.

Here, we performed RNA bisulfite sequencing (RNA-Bis-seq) on EBV-infected NPC cells to systematically identify the RNA m^{5}C writers and readers involved in EBV-induced RNA modifications. Integrating transcriptomic analysis with functional validation experiments, we demonstrate that EBV-encoded LMP1 significantly upregulates the RNA m^{5}C writer NSUN2. NSUN2 subsequently catalyzes the RNA m^{5}C modification of ICAM-1 mRNA, facilitating recruitment of the newly identified m^{5}C reader protein YBX3 and its partner PABPC1, thereby promoting ICAM-1 translation and NPC metastasis. Our findings uncover a previously unrecognized mechanism by which EBV promotes tumor progression and establish the NSUN2/YBX3/m^{5}C-ICAM-1 signaling axis as a potential therapeutic target for NPC.

MATERIALS AND METHODS

Clinical samples

For scRNA-seq, 10 NPC samples were collected at the Sun Yat-sen University Cancer Center (SYSUCC, Guangzhou, China) between June 2018 and September 2018, as previously reported [20]. For bulk RNA-Seq, tumor biopsy specimens from 95 NPC patients were collected at SYSUCC, while another independent cohort of 113 NPC tumor biopsy samples was obtained from a previously published study [21]. For IHC analysis, paraffin-embedded NPC tissues ($n = 100$) were collected at SYSUCC between September 2010 and March 2020. All cases were classified according to the World Health Organization Histological Typing (WHOHT) criteria.

Statistical analysis

Statistical analyses were performed using GraphPad Prism 7.0. Survival curves were generated using the Kaplan-Meier method and compared using the log-rank test. Pearson correlation analysis was conducted to assess correlations between different genes. Statistical significance was determined using a two-tailed Student's *t* test for comparisons between two groups and one-way analysis of variance (ANOVA) for comparisons involving more than two groups. A *P*-value of <0.05 was considered statistically significant. All histograms represent mean values ± standard deviation (SD) derived from at least three independent experiments.

RESULTS

EBV infection enhances RNA m^{5}C modification by LMP1-mediated NSUN2 elevation in NPC

To investigate the role of RNA m^{5}C modification in EBV-associated NPC, we conducted integrated RNA bisulfite sequencing (RNA-Bis-seq) analyses on HK-1 NPC cells infected with EBV in vitro (see Methods). RNA-Bis-seq revealed a significant global increase in RNA m^{5}C modifications following EBV infection (Fig. 1A). To identify key regulators responsible for the increased RNA m^{5}C modifications, we analyzed the expression of classical RNA m^{5}C "writers" (NSUN1-NSUN7) [22], and observed significant transcriptional upregulation of NSUN2 in EBV-infected NPC cells (Fig. 1B and Supplementary Fig. 1A). qPCR and western blot analyses confirmed elevated NSUN2 expression at both mRNA and protein levels (Fig. 1C, D). Single-cell RNA sequencing (scRNA-seq) analysis further demonstrated significantly higher NSUN2 expression in malignant NPC cells exhibiting high EBV gene activity (EBV-high) compared to EBV-low cells (see Methods; Fig. 1E and Supplementary Fig. 1B). Consistent with these findings, correlation analysis using clinical NPC samples indicated a strong positive association between NSUN2 expression and EBV gene activation [23] (Supplementary Fig. 1C). Importantly, NSUN2 knockdown markedly decreased global RNA m^{5}C modification level in HK-1-EBV and CNE2-EBV cells, whereas its overexpression enhanced m^{5}C modification (Fig. 1F and Supplementary Fig. 1D). Collectively, these findings suggest that NSUN2 is a crucial mediator of EBV-induced RNA m^{5}C modifications in NPC.

To explore the mechanism underlying EBV-induced NSUN2 upregulation, we examined correlations between NSUN2 and EBV-encoded genes. Among these, LMP1 exhibited the strongest correlation with NSUN2 expression (Fig. 1G and Supplementary Fig. 1E). Furthermore, LMP1 overexpression significantly enhanced NSUN2 expression at both mRNA and protein levels in HK-1-EBV and CNE2-EBV cells (Fig. 1H, I). Consistently, dot blot analysis revealed that LMP1 knockdown significantly reduced, whereas LMP1 overexpression markedly enhanced, the global RNA m^{5}C modification levels in EBV-positive NPC cells (Supplementary Fig. 1F). These data strongly suggest that EBV-encoded LMP1 promotes NSUN2 elevation in NPC.

To identify the signaling pathways mediating LMP1-regulated NSUN2, we conducted bulk RNA sequencing on NPC cells with LMP1 knockdown or overexpression (Supplementary Fig. 2A). Pathway enrichment analysis of differentially expressed genes resulting from LMP1 overexpression revealed gene enrichment in interferon response, NF-κB signaling, JAK/STAT3 signaling, and KRAS signaling pathways (Supplementary Fig. 2B). Transcriptional correlation analysis demonstrated significant positive correlation between NSUN2 expression and NF-κB pathway activation in NPC tissues (Fig. 1J and Supplementary Fig. 2C). Moreover, Gene Set Enrichment Analysis (GSEA) confirmed that NF-κB pathway was significantly upregulated in NPC cells overexpressing LMP1, and this upregulation was reduced upon LMP1 knockdown (Supplementary Fig. 2D). Consistently, treatment with NF-κB pathway inhibitor (PTDC) or knockdown of NF-κB or LMP1 significantly attenuated LMP1-induced NSUN2 expression (Fig. 1K and Supplementary Fig. 2E). Together, these findings strongly suggest that LMP1 upregulates NSUN2 through NF-κB signaling, enhancing global RNA m^{5}C modifications in NPC.

NSUN2 regulates tumor metastasis through its RNA m^{5}C catalytic activity

To assess the biological impact of EBV-induced RNA m^{5}C modifications, we performed GSEA and Gene Ontology (GO) analyses of the RNA-Bis-seq data. These analyses revealed that genes with elevated m^{5}C modification levels after EBV infection were significantly enriched in cell migration and metastasis pathways (Fig. 2A and Supplementary Fig. 3A). To confirm the role of NSUN2 catalytic activity in tumor metastasis, we generated NSUN2 knockdown in EBV-positive NPC cell lines (HK-1-EBV and CNE2-EBV) and performed rescue experiments with either wild-type NSUN2 (WT) or a double-mutant (DM) lacking functional catalytic m^{5}C sites (Cys271 and Cys321; Supplementary Fig. 3B, C). Strikingly, NSUN2 knockdown significantly reduced NPC cell invasion and migration, and this inhibitory phenotype was reversed by re-expression of the WT-NSUN2 but not by the mutant DM-NSUN2 (Fig. 2B).

Consistently, a series of in vivo metastasis mouse models demonstrated that NSUN2 knockdown markedly inhibited NPC metastases to lymph node, lung and liver, which was reversed by the WT-NSUN2, but not the catalytic mutant (Fig. 2C-I and Supplementary Fig. 3D). Notably, EBV infection alone was insufficient to promote cell migration in the absence of NSUN2, highlighting the essential role of NSUN2 in EBV-driven NPC metastasis (Supplementary Fig. 3E). Collectively, these findings firmly establish that NSUN2 contributes to EBV-induced NPC metastasis through its RNA m^{5}C catalytic activity.

YBX3 is a novel RNA m^{5}C reader mediating EBV-induced metastasis

To identify RNA m^{5}C readers involved in EBV-induced metastasis, we initially evaluated known readers, including ALYREF, YBX1, YBX2, SRSF2, and LIN28B. These genes showed minimal or

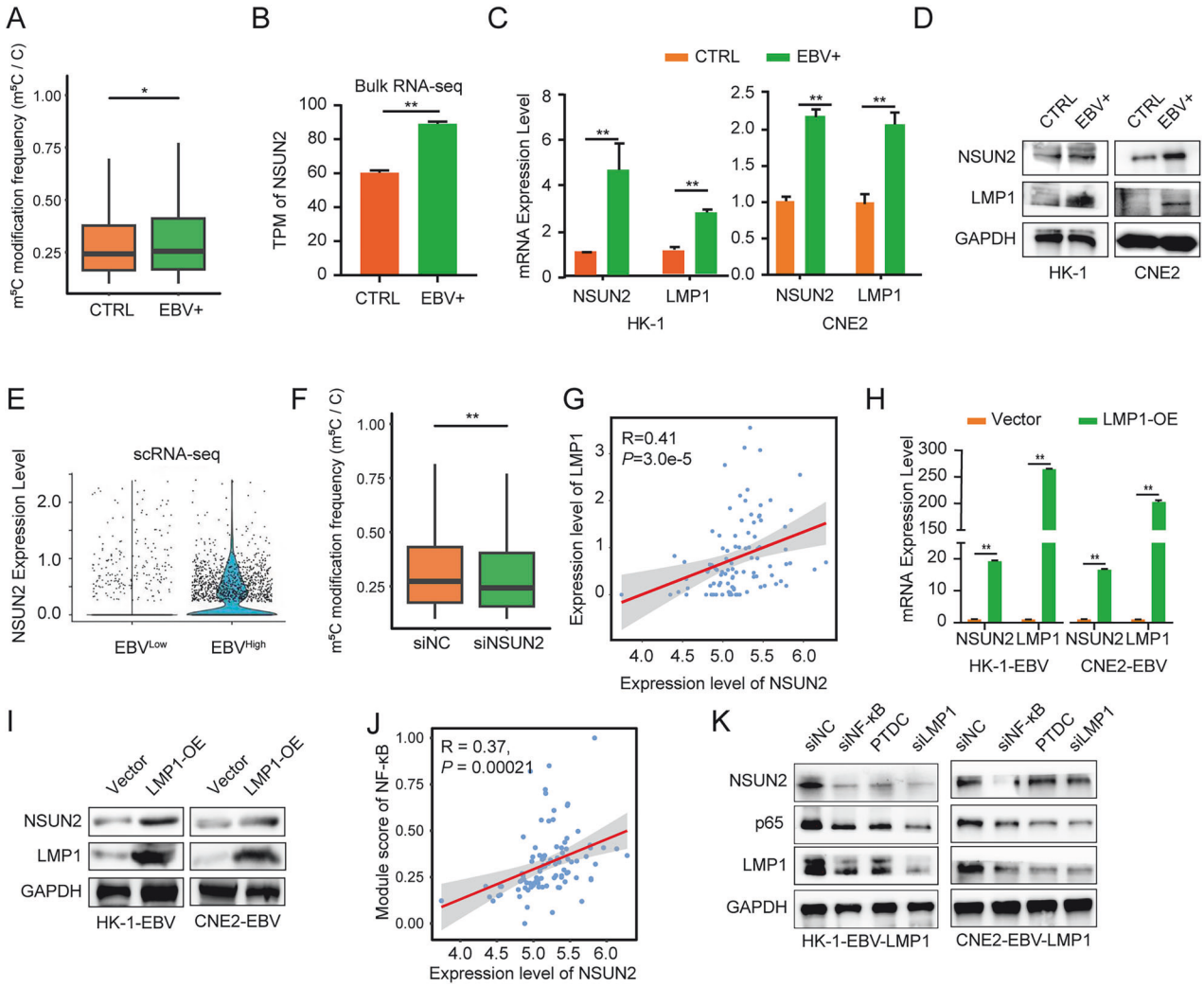

Fig. 1 EBV infection enhances RNA m^{5}C level through upregulating NSUN2 in NPC. A RNA-Bis-seq analysis demonstrating overall upregulation of RNA m^{5}C modification in EBV-infected HK-1 cells (EBV +) compared with parental control cells (CTRL). **B** RNA-seq analysis showing the upregulated NSUN2 transcription level in EBV + HK-1 cells described in A. TPM: Transcripts Per Million. Data are the mean ± SD. NSUN2 expression levels in HK-1 and CNE2 cells before (CTRL) and after EBV infection (EBV +) at mRNA and protein levels as determined by qPCR (**C**) and western blot analysis (**D**), respectively. LMP1 serves as a reference. Data are the mean ± SD. **E** Single-cell transcriptome analysis revealing higher NSUN2 transcription levels in EBV high (EBV^{high}) than low (EBV^{low}) cell clusters of malignant cells in NPC clinical samples ($n = 10$). Cells without EBV transcription detected by scRNA-seq are defined as EBV low; otherwise, EBV high. **F** RNA-Bis-seq analysis demonstrating overall downregulation of RNA m^{5}C modification in HK-1-EBV cells with NSUN2 knockdown (siNSUN2) compared with control cells (siNC). **G** Transcriptional correlation between NSUN2 and EBV-encoded LMP1 in NPC samples ($n = 95$). NSUN2 expression levels in HK-1-EBV and CNE2-EBV cells with LMP1 overexpression (LMP1-OE) or without (Vector) as determined by qPCR (**H**) and western blot analysis (**I**). Data are the mean ± SD. **J** Transcriptional correlation between NSUN2 and NF-κB signaling pathway in NPC samples ($n = 95$). **K** Western blot analysis evaluating the protein levels of NSUN2, NF-κB-p65, and LMP1 in HK-1-EBV and CNE2-EBV cells overexpressing LMP1 with or without blocking NF-κB signaling pathway using the pathway inhibitor (PTDC) or siRNA (siNF-κB). Representative western blot images of three biological replicates with similar results are shown in (**D**, **I**, **K**). Data in (**C**, **H**) are Mean ± SD from three independent experiments. Statistical analyses were performed using appropriate tests based on data distribution: two-sided unpaired Student's *t* test was applied for (**A**, **B**, **C**, **F**, **H**) and correlation analyses for (**G**, **J**) were conducted using the cor. test function in R (v4.4.2). *$P < 0.05$, ** $P < 0.01$.

undetectable expression in EBV-infected cells and scRNA-seq datasets (Supplementary Fig. 4A, B). Given that YBX1 and YBX2 are established RNA m^{5}C readers from the YBX family [24, 25]. We hypothesized that YBX3, a related protein, might also function similarly. Sequence alignment analysis revealed a high degree of structural conservation across YBX family members, particularly in the cold shock domain (CSD) and a putative m^{5}C binding site (Fig.3A, B). RNA pull-down and electrophoretic mobility shift assays (EMSA) demonstrated that YBX3 binds specifically to m^{5}C-modified RNA oligos with affinity comparable to YBX1 (Fig. 3C, D and Supplementary Fig. 4C). Additionally, nucleic acid mass spectrometry analysis further confirmed significantly higher m^{5}C levels in YBX3-bound RNAs compared to control samples (Fig. 3E), strongly suggesting YBX3 as a novel RNA m^{5}C reader.

To explore the link between EBV infection and YBX3 expression, we performed transcriptomic analysis and revealed upregulated YBX3 expression in EBV-infected cells (Supplementary Fig. 4D), which was validated by qPCR and western blot assays at both mRNA and protein levels, respectively (Fig. 3F, G). Furthermore, scRNA-seq analysis revealed that YBX3 was remarkably upregulated in EBV-positive NPC cells (Supplementary Fig. 4E). Moreover, correlation analysis revealed a strong association between LMP1 and YBX3 expression in NPC samples (Supplementary Fig. 4F). Additionally, LMP1 overexpression significantly induced YBX3

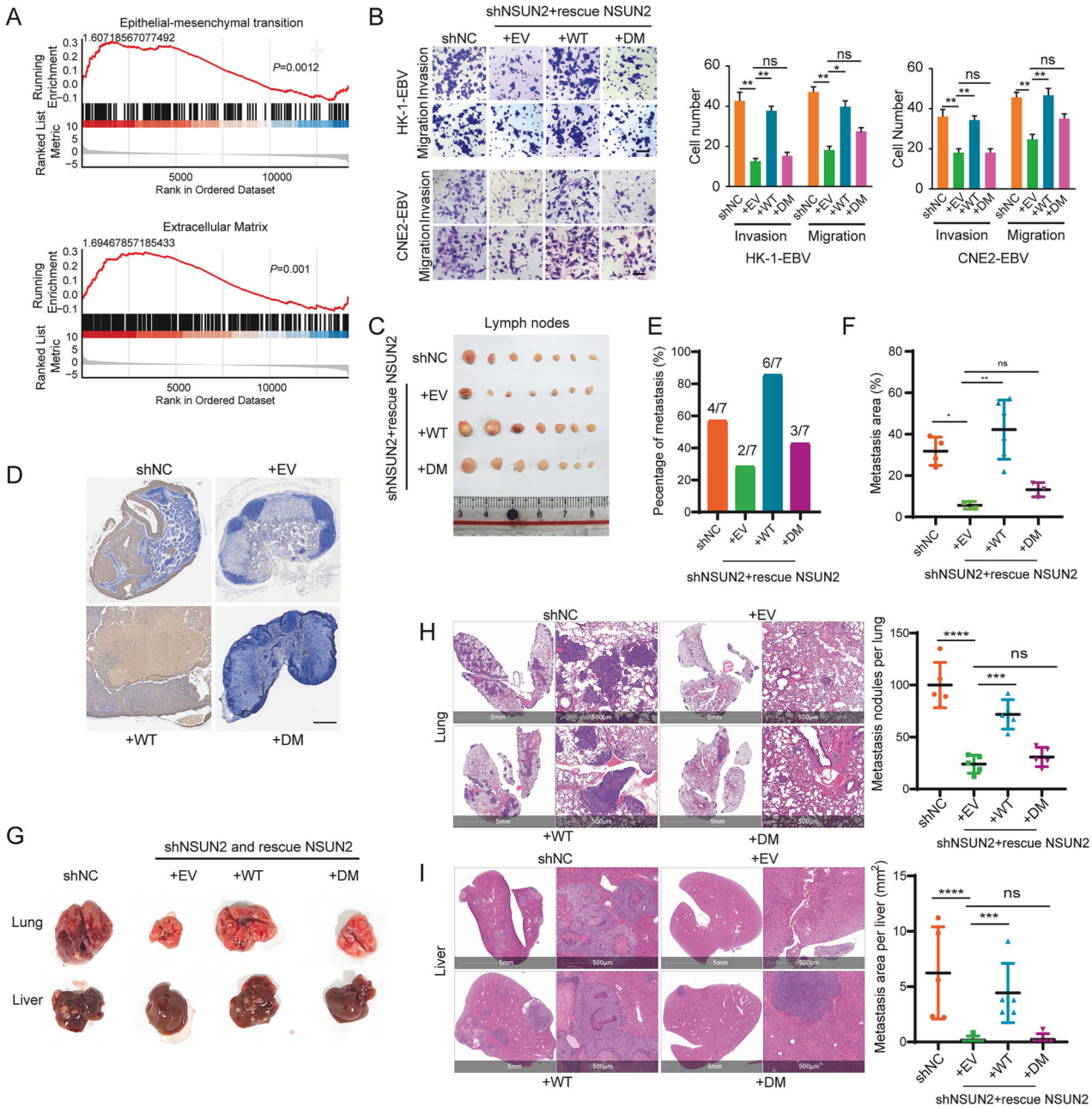

Fig. 2 NSUN2 promotes NPC metastasis through its RNA m^{5}C catalytic ability. A Gene Set Enrichment Analysis (GSEA) analysis of RNA m^{5}C up-regulated genes revealing upregulated EMT-related pathways in EBV-infected HK-1 cells. **B** Transwell assays showing the invasion and migration abilities of HK-1-EBV and CNE2-EBV cells with NSUN2 knockdown using shRNA lentivirus while transiently rescuing wide-type NSUN2 (WT), mutant lacking m^{5}C catalytic site Cysteine 271 (C271) and Cysteine 321 (C321) determined as double mutant (DM), and empty vector (EV) as control. Representative images of three biological replicates with similar results were shown. **C** Lymph node metastasis from mice ($n = 7$ mice/group) with foot-pad inoculation of CNE2-EBV cells described in B. Extracted lymph nodes were imaged after one month of inoculation. **D** IHC staining of pan-CK antibodies showing tumor metastasis in lymph nodes displayed in C. Scale bar, 500 μm. Percentages (**E**) and areas (**F**) of metastasis in lymph nodes in (**C**). **G** Representative images of the lung and liver from mice ($n = 5$ mice/group) intravenously injected with CNE2-EBV cells described in (**B**). Hematoxylin and eosin (HE) staining of lung (**H**) and liver (**I**) tissue sections from (**G**), with statistical analysis of metastasis rates presented on the right. Statistical analyses were performed using appropriate tests based on data distribution: the one-way ANOVA test was used for (**B**, **F**, **H**, **I**). *$P < 0.05$, ** $P < 0.01$, *** $P < 0.001$, **** $P < 0.0001$.

expression in NPC cells (Fig. 3H, I). These findings strongly suggest that YBX3 mediates EBV-driven activities in NPC.

To assess the functional role of YBX3 in NPC metastasis, we established NPC-EBV cell lines with YBX3 knockdown, followed by rescue with either wild-type YBX3 (WT) or mutant YBX3 lacking the RNA m^{5}C binding site (MUT; Fig. 3J). YBX3 knockdown dramatically reduced NPC cell migration, while reintroducing wild-type but not the m^{5}C-binding-deficient mutant YBX3 fully restored migration ability (Fig. 3J, K). Collectively, these findings demonstrate that YBX3 functions as a critical RNA m^{5}C reader to promote EBV-induced NPC metastasis.

NSUN2 and YBX3 jointly regulate m^{5}C modification of ICAM-1 to enhance its translation

To explore the mechanism by which NSUN2-mediated RNA m^{5}C modification contributes to NPC metastasis, we analyzed RNA-Bis-

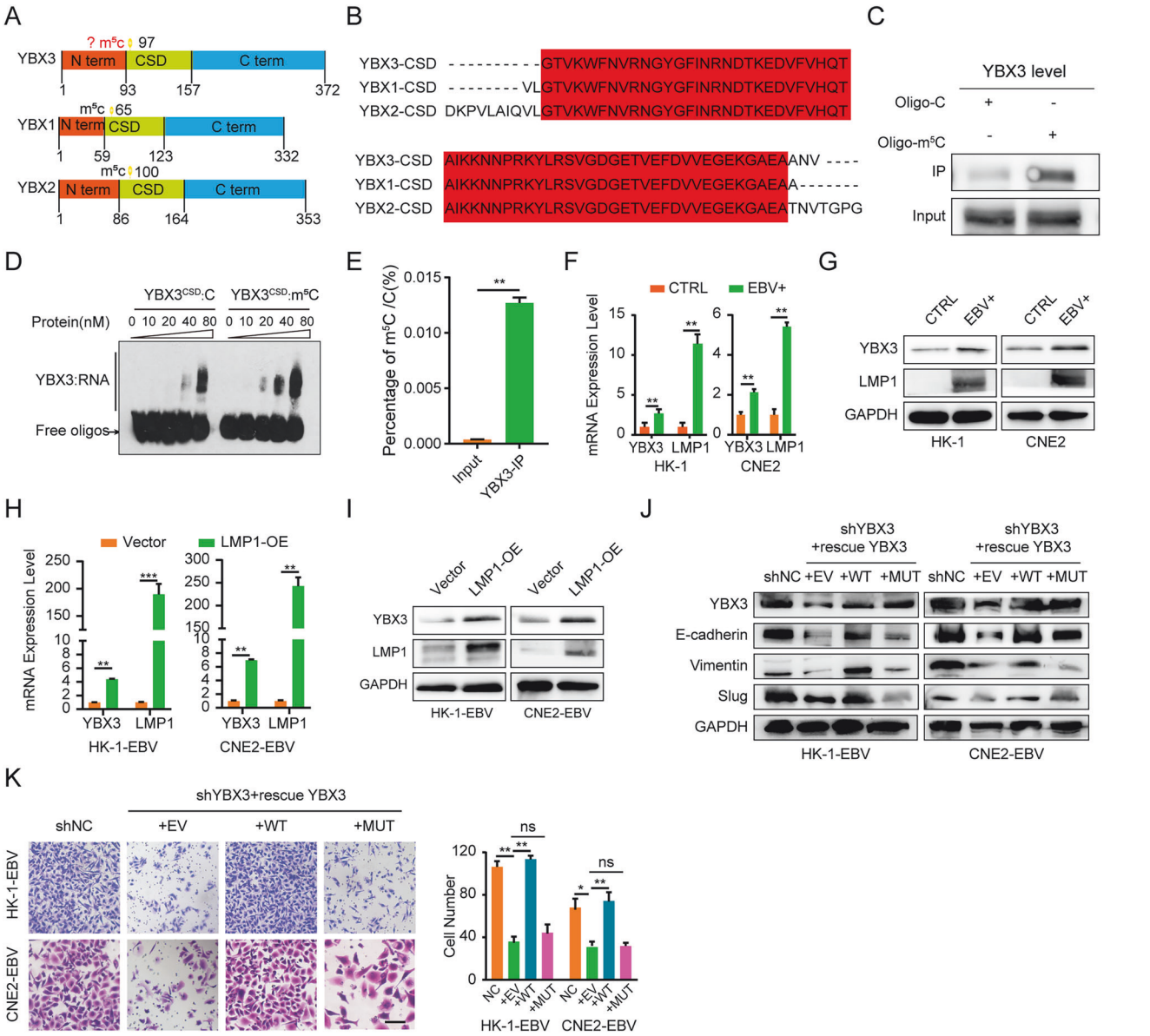

Fig. 3 YBX3 is a novel RNA m^{5}C binding protein responding to EBV infection. A Schematic presentation of the functional domains for the YBXs' family members. CSD, cold shock domain. **B** Alignment of amino acid sequence of the cold shock domain across YBXs' family members. Conserved regions are highlighted in red. **C** Western blot assays showing YBX3 protein levels pulled down by biotin-labeled oligo-C or oligo-m^{5}C RNA probes in HK-1-EBV cells. **D** Electrophoretic Mobility Shift Assay (EMSA) showing the binding ability of YBX3 cold shock domain (CSD) protein (YBX3^{CSD}) with oligo-C or oligo-m^{5}C RNA probes. **E** High Performance Liquid Chromatography (HPLC) detecting the RNA m^{5}C level in total (input) or YBX3-bound RNAs (YBX3-IP). YBX3 and LMP1 expression in HK-1 and CNE2 cells before (CTRL) and after EBV infection (EBV +) as determined by qPCR (**F**) and western blot analysis (**G**), respectively. YBX3 and LMP1 expression in HK-1-EBV and CNE2-EBV cells with (LMP1-OE) or without (Vector) LMP1 overexpression as determined by qPCR (**H**) and western blot analysis (**I**), respectively. **J** Western blot analysis evaluating the expression of YBX3 and EMT-related markers in HK-1-EBV and CNE2-EBV cells. Cells were knocked down of YBX3 by shRNA lentivirus and rescued with transient transfection of wild-type YBX3 (WT), mutant lacking m^{5}C modification binding site (MUT), and empty vector (EV) as control. Cells without YBX3 knockdown were scrambled. **K** Transwell assays assessing the migration abilities of cells described in (**J**), with statistic of three biological replicates presented on the right. Scale bar, 50 μm. Representative western blot images of three biological replicates with similar results are shown in (**C**, **D**, **G**, **I**, **J**). Data in (**E**, **F**, **H**) are Mean ± SD from three independent experiments. Statistical analyses were performed using appropriate tests based on data distribution: two-sided unpaired Student's *t* test was applied for (**E**, **F**, **H**), and one-way ANOVA test was used for (**K**). *$P < 0.05$, ** $P < 0.01$, *** $P < 0.001$.

seq data and identified 81 genes with both elevated RNA m^{5}C levels upon EBV infection and reduced m^{5}C levels following NSUN2 knockdown (Fig. 4A). GO analysis revealed that these overlapping genes were significantly enriched in pathways related to metastasis and viral infection (Supplementary Fig. 5A), highlighting three key genes—ICAM-1, SLC7A1, and CHST2 (Supplementary Fig. 5B). Among these, ICAM-1 exhibited the strongest positive correlation with NSUN2 expression in clinical NPC samples (Supplementary Fig. 5C). Furthermore, transcriptomic analysis revealed a significant positive correlation between ICAM-1 expression and EBV gene expression, with LMP1 exhibiting the most prominent association (Supplementary Fig. 5D, E). These results suggest ICAM-1 as a primary target of NSUN2 regulation upon EBV infection.

To confirm how NSUN2 catalyzes the m^{5}C modification of ICAM-1 RNA, we performed m^{5}C RNA immunoprecipitation followed by

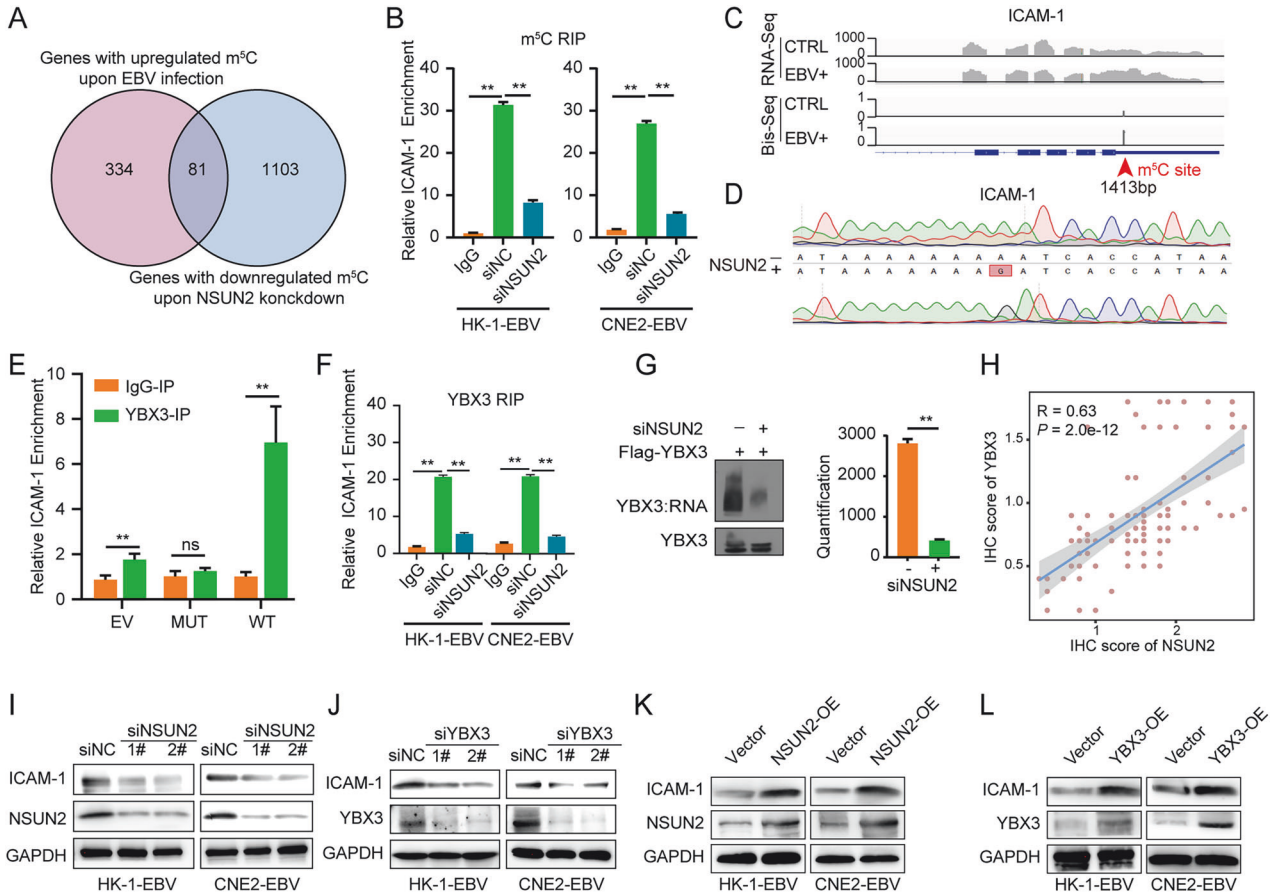

Fig. 4 NSUN2 and YBX3 jointly promote the m^{5}C modification of ICAM-1. A Diagram showing the number of overlap genes with upregulated m^{5}C modification levels induced by EBV infection and those with downregulated levels upon NSUN2 knockdown. **B** m^{5}C RIP assays revealing m^{5}C modification level of ICAM-1 with (siNSUN2) or without (siNC) NSUN2 knockdown in NPC cells. IgG-IP was used as control. **C** RNA-Seq and Bis-Seq analyses of ICAM-1 in EBV-infected NPC cells, highlighting the m^{5}C modification site (red arrow). **D** In vitro methylation assays assessing the catalytic activity of NSUN2 protein on the specific m^{5}C modification site of ICAM-1 using the bisulfite conversion method. The red box indicates the m^{5}C modification site. **E**, **F** RIP-qPCR assays revealing the binding ability of YBX3 with ICAM-1 RNA in NPC cells. HK-1-EBV cells were transfected with wild-type (WT) or catalytic mutant (MUT) YBX3 plasmids. HK-1-EBV and CNE2-EBV cells were knocked down for NSUN2 (siNSUN2) or not (siNC); IgG-IP was used as a control. **G** Western blot revealing RNA binding ability of YBX3 in the presence (siNSUN2-) or absence of NSUN2 (siNSUN2 +) in HK-1-EBV cells with FLAG-YBX3 overexpression. Quantification statistics of RNA levels bound to YBX3 protein are presented on the right. **H** Correlation of protein expression between YBX3 and NSUN2 in NPC tissues ($n = 100$). Western blot analysis assessing the expression level of ICAM-1 in HK-1-EBV and CNE2-EBV cells transfected with NSUN2 (**I**) or YBX3 (**J**) siRNAs, or infected with lentivirus overexpressing NSUN2 (**K**) or YBX3 (**L**). Representative western blot images of three biological replicates with similar results are shown in (**G**, **I**, **J**, **K**, **L**). Data in (**B**, **E**, **F**, **G**) are Mean ± SD from three independent experiments. Statistical analyses were performed using appropriate tests based on data distribution: two-sided unpaired Student's *t* test was applied for (**E**, **G**), one-way ANOVA test was used for (**B**, **F**), and correlation analyses for (**H**) were conducted using the cor. test function in R. *$P < 0.05$, ** $P < 0.01$.

qPCR (m^{5}C RIP-qPCR) analysis, revealing a significant enrichment of ICAM-1 RNA in NSUN2-immunoprecipated samples (Fig. 4B and Supplementary Fig. 5F). RNA-Bis-seq analysis further identified a specific m^{5}C site (C base) at 1413 bp on ICAM-1 mRNA (Fig. 4C). Consistently, in vitro methylation assays confirmed that bisulfite treatment could convert C base at this position to T base, indicating its unmethylated state (Fig. 4D, upper). In contrast, the addition of recombinant NSUN2 protein prevented this conversion, demonstrating that NSUN2 directly catalyzes m^{5}C methylation at this specific site on ICAM-1 mRNA (Fig. 4D, bottom).

RIP-qPCR using YBX3 antibodies demonstrated that YBX3 directly binds to ICAM-1 RNA (Supplementary Fig. 5G), an interaction significantly impaired upon YBX3 mutation lacking the m^{5}C-binding domain or NSUN2 knockdown (Fig. 4E, F). Moreover, EMSA showed that NSUN2 knockdown markedly reduced YBX3's binding affinity to ICAM-1 RNA in HK-1-EBV cells (Fig. 4G). Supportively, correlation analysis in clinical NPC samples indicated a significant positive association between NSUN2 and YBX3 protein levels (Fig. 4H). Collectively, these findings demonstrate that NSUN2-mediated m^{5}C modification of ICAM-1 RNA facilitates YBX3 binding, establishing a coordinated regulatory axis involving the RNA m^{5}C writer NSUN2 and reader YBX3.

Previous studies have shown that RNA m^{5}C modifications can affect diverse cellular processes, including RNA stability and translation [26–28]. To clarify whether NSUN2 and YBX3 regulate ICAM-1 RNA stabilization, we treated NPC cells with actinomycin-D, a transcription inhibitor, and measured the half-life of ICAM-1 mRNA. Interestingly, knockdown of either NSUN2 or YBX3 did not significantly affect ICAM-1 mRNA stability (Supplementary Fig. 5H). However, knockdown of either NSUN2 or YBX3 significantly reduced ICAM-1 protein levels (Fig. 4I, J), while their overexpression markedly increased ICAM-1 protein abundance (Fig. 4K, L). These results indicate that NSUN2 and YBX3 predominantly regulate ICAM-1 expression at the translational level, rather than by modulating mRNA stability.

YBX3 recruits PABPC1 to enhance ICAM-1 translation

Given that RNA m^{5}C reader proteins commonly interact with partner proteins to regulate post-transcriptional processes [28].

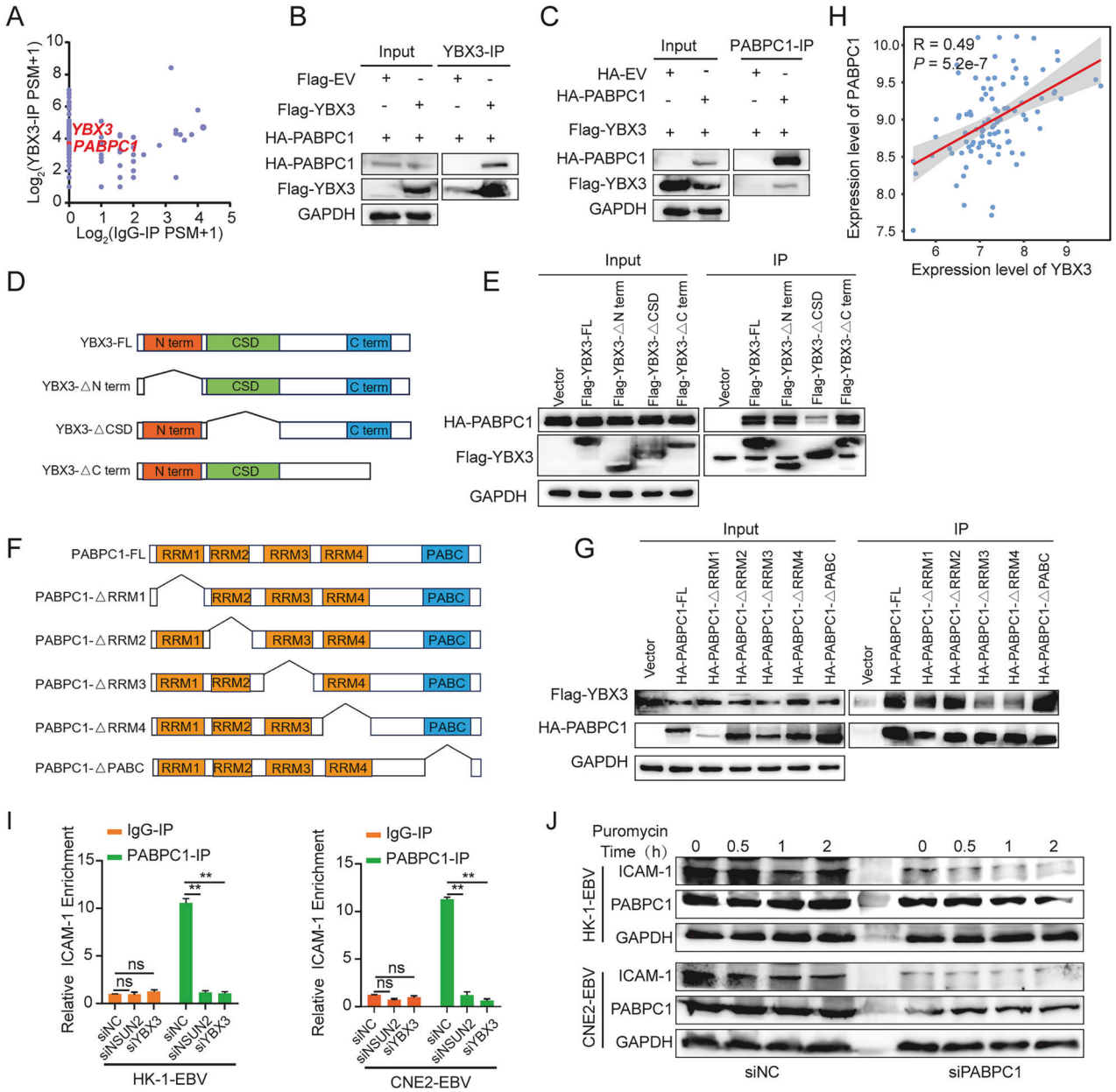

Fig. 5 YBX3 recruits PABPC1 to regulate ICAM-1 translation. A Scatter plot of proteins bound to YBX3 or IgG in HK-1-EBV cells. X-axis presents the peptide number bound to IgG, while y-axis shows the peptide number bound to YBX3. PSM, the peptide-spectrum matches. YBX3 and its protein partner PABPC1 are highlighted in red. **B**, **C** Co-immunoprecipitation (Co-IP) assays showing the interaction between YBX3 and PABPC1 in 293T cells. Cells were transfected with Flag-YBX3 and/or HA-PABPC1 plasmids as indicated. The immunoprecipitation efficiency and enriched FLAG-YBX3 or HA-PABPC1 were detected by immunoblotting with antibodies against FLAG and HA, respectively. Schematic diagram showing domain structures of wild-type and mutant constructs of YBX3-FLAG (**D**) and HA-PABPC1 (**F**). Co-IP assays in 293T cells co-transfected with either wild-type or mutant combination of HA-PABPC1 and FLAG-YBX3. Immunoprecipitations were performed with anti-FLAG (**E**) anti-HA (**G**) antibodies. IP, immunoprecipitation. **H** Transcriptional correlation between YBX3 and PABPC1 in NPC samples ($n = 95$). Correlation coefficient and P value were calculated using the 'cor. test' function in R. **I** RIP-qPCR assay detecting PABPC1's binding level to ICAM-1 in HK-1-EBV and CNE2-EBV cells with NSUN2 (siNSUN2) or YBX3 (siYBX3) knockdown, compared to control cells (siNC). IgG-IP was used as a control. Data are the mean ± SD. **J** Western blot analysis evaluating ICAM-1 protein expression in HK-1-EBV and CNE2-EBV cells with PABPC1 knockdown by siRNA and concurrently treated with puromycin. Representative western blot images of three biological replicates with similar results are shown in (**B**, **C**, **E**, **G**, **J**). Data in (**I**) are Mean ± SD from three independent experiments. Statistical analyses were performed using appropriate tests based on data distribution: correlation analyses for (**H**) were conducted using the cor. test function in R; and one-way ANOVA test was used for (**I**). *$P < 0.05$, ** $P < 0.01$.

We performed immunoprecipitation coupled with mass spectrometry (IP-MS) using YBX3-specific antibodies to identify potential interacting partners involved in YBX3-mediated m^5C functions. Supportively, GO analysis of YBX3-associated proteins revealed a significant enrichment in pathways related to protein translation (Supplementary Fig. 6A). Notably, PABPC1 emerged as the most abundant YBX3-interacting protein identified (Fig. 5A). To validate this interaction, we conducted co-immunoprecipitation (co-IP) assays using antibodies specific to either YBX3 or PABPC1, confirming their direct interaction in NPC cells (Fig. 5B, C). Co-IP assays with a series of domain-deletion mutants showed that CSD deletion in YBX3 (YBX3-FLAG-ΔCSD) obviously abolished

interaction with PABPC1 (Fig. 5D, E). Similarly, PABPC1 lacking the third and fourth RRM domains (PABPC1-HA-ΔRRM3 and PABPC1-HA-ΔRRM4) failed to interact with YBX3 (Fig. 5F, G). These results indicate that the CSD domain of YBX3 and the two RRM domains of PABPC1 are critical for their interaction. Additionally, correlation analysis of clinical NPC samples demonstrated a significant positive association between YBX3 and PABPC1 expression levels (Fig. 5H).

Considering the established role of PABPC1 in regulating mRNA translation [29–31]. We investigated whether PABPC1 directly interacts with ICAM-1 mRNA. RIP-qPCR assays confirmed significant enrichment of ICAM-1 RNA in PABPC1-bound fractions in NPC-EBV cells (Supplementary Fig. 6B). Importantly, this interaction was significantly abolished upon knockdown of either NSUN2 or YBX3 (Fig. 5I). Furthermore, PABPC1 knockdown markedly reduced ICAM-1 protein levels (Supplementary Fig. 6C, D). Consistently, a puromycin incorporation assay, indicative of global translational activity, revealed that PABPC1 depletion significantly inhibited ICAM-1 mRNA translation in NPC cells (Fig. 5J and Supplementary Fig. 6E). Collectively, these findings demonstrate that YBX3 recruits PABPC1 to ICAM-1 mRNA, enhancing its translation, thus highlighting a key functional axis by which RNA m^5C modifications promote NPC metastasis.

RNA m^5C modification of ICAM-1 mediates NSUN2-induced NPC metastasis

To determine the functional significance of RNA m^5C modification on ICAM-1 in NPC metastasis, we generated NPC-EBV cell lines with stable ICAM-1 knockdown, followed by rescue expression using either wild-type ICAM-1 (WT) or an ICAM-1 mutant lacking the m^5C modification site (MUT; Supplementary Fig. 7A). ICAM-1 knockdown significantly impaired NPC cells' migration, a defect fully reversed by introducing WT-ICAM-1. In contrast, the m^5C-deficient ICAM-1 mutant (MUT) failed to rescue migration (Fig.6A), underscoring the essential role of RNA m^5C modification in ICAM-1-mediated metastasis. To further assess whether ICAM-1 acts downstream of NSUN2 in promoting NPC metastasis, we performed rescue experiments by overexpressing ICAM-1 in NSUN2-knockdown NPC cells. Transwell assays demonstrated that ICAM-1 overexpression significantly reversed the migration defects induced by NSUN2 knockdown, achieving an effect comparable to direct NSUN2 re-expression (Fig. 6B). These findings were further corroborated by in vivo lymph node, lung and liver metastasis models, where NSUN2 knockdown markedly reduced NPC metastasis, while re-expression of either NSUN2 or ICAM-1 fully restored metastatic capacity (Fig. 6C–G and Supplementary Fig. 7B). These results demonstrate ICAM-1 as a critical effector downstream of NSUN2 in promoting NPC metastasis through RNA m^5C modification.

Next, we examined the clinical significance of the identified NSUN2/YBX3/ICAM-1 signaling axis in NPC. Transcriptomic analysis revealed that NSUN2, YBX3, and ICAM-1 were significantly elevated in NPC tumor samples compared to normal tissues (Supplementary Fig. 7C). Immunohistochemistry (IHC) assays confirmed predominant tumor-specific expression of NSUN2, YBX3, and ICAM-1 (Fig. 7A). Additionally, correlation analysis demonstrated a strong association between high ICAM-1 protein levels and elevated NSUN2 and YBX3 expression in NPC tissues (Fig. 7B). Importantly, elevated expression levels of these three genes correlate with advanced tumor stages and lymph node metastasis (N stages) in NPC patients (Fig. 7C, D and Supplementary Fig. 7D). Kaplan-Meier survival analysis also revealed that NPC patients with high expression of NSUN2, YBX3, or ICAM-1 had a poorer prognosis, with the combined upregulation of all three genes in 29% cases demonstrating the most significant prognostic impact (Fig. 7E). These data collectively suggest that the integrated activity of the NSUN2/YBX3/ICAM-1 axis critically contributes to NPC progression and prognosis.

DISCUSSION

EBV infection is a major etiological factor contributing to NPC pathogenesis. Previous studies have shown that EBV influences gene regulation at multiple regulatory levels, including transcriptional, post-transcriptional, and post-translational processes [15, 32–34]. In this study, we demonstrate, for the first time to our knowledge, that EBV infection globally increases RNA m^5C modifications in NPC by specifically upregulating NSUN2, a well-established RNA m^5C methyltransferase [10]. NSUN2 has been previously implicated in promoting tumor progression and resistance to anti-PD-L1 immunotherapy across various malignancies [35–37]. However, its precise mechanisms of activation and tumor-promoting functions in EBV-associated NPC have remained unclear. Our findings reveal that EBV encoding LMP1 drives NSUN2 upregulation through NF-κB signaling, an oncogenic pathway frequently activated in NPC [38, 39]. Functional assays further corroborate that NSUN2 promotes NPC cell metastasis in an RNA m^5C-dependent manner, and silencing NSUN2 effectively reverses the pro-metastatic phenotypes induced by EBV infection. Collectively, these findings define a novel EBV-NSUN2-m^5C regulatory axis, underscoring the critical role of RNA m^5C modification in EBV-associated NPC metastasis.

RNA modifications represent a diverse class of epitranscriptomic marks, which typically exert their biological functions through recognition by specific RNA-binding proteins, termed "readers", to modulate downstream cellular processes [40]. Here, we identify YBX3 as a novel RNA m^5C reader that specifically recognizes EBV-induced m^5C modifications. YBX3 is a DNA/RNA-binding protein previously linked to transcriptional regulation of genes involved in DNA repair and implicated in various diseases [41]. We found that YBX3 contains a highly conserved cold shock domain (CSD), a structural motif essential for m^5C-RNA binding, shared by classical m^5C readers within the YBX family (YBX1 and YBX2) [24, 25]. Biochemical assays confirmed that YBX3 binds to m^5C-modified transcripts with high binding affinity, establishing its functionality as a genuine RNA m^5C reader. Furthermore, functional experiments demonstrated that YBX3 promotes NPC metastasis through its m^5C-binding ability, consistent with previously reported oncogenic roles of YBX3 in multiple malignancies, including colon cancer [42], kidney renal clear cell carcinoma [43], leukaemia [44], hepatocarcinoma [45], and NPC [46]. Collectively, these findings expand the functional landscape of YBX3, identifying it as a critical RNA m^5C reader involved in EBV-associated NPC metastasis.

We further identified ICAM-1 as a critical downstream target regulated by the NSUN2/YBX3-mediated RNA m^5C modification pathway in NPC metastasis. ICAM-1 is a cell adhesion molecule widely implicated in facilitating metastatic dissemination across various cancer types [47–51]. In NPC, previous studies reported that LMP1 promotes cell migration through ICAM-1 upregulation [52, 53]. However, the detailed molecular mechanisms underlying this regulatory relationship have remained unclear. Here, we uncover a novel m^5C-dependent mechanism whereby NSUN2 catalyzes m^5C modification of ICAM-1 mRNA, enabling its specific recognition by the m^5C reader protein YBX3. Subsequently, YBX3 recruits the translation-promoting factor PABPC1 to the m^5C-modified site, thereby enhancing ICAM-1 translation. Functional assays confirmed that ICAM-1 acts as a crucial mediator in NSUN2-driven NPC metastasis in an RNA m^5C-dependent manner. Together, our findings elucidate how EBV hijacks the host RNA modification machinery to drive NPC metastasis via the NSUN2-YBX3-ICAM-1 axis.

Moreover, we observed significant upregulation of NSUN2, YBX3, or ICAM-1 in NPC tumor tissues, and their elevated expression correlated with poor prognosis. These findings indicate that the NSUN2/YBX3/ICAM-1 regulatory axis may serve as a crucial prognostic biomarker and a potential therapeutic target in NPC. Currently, NPC treatment primarily relies on radiation and

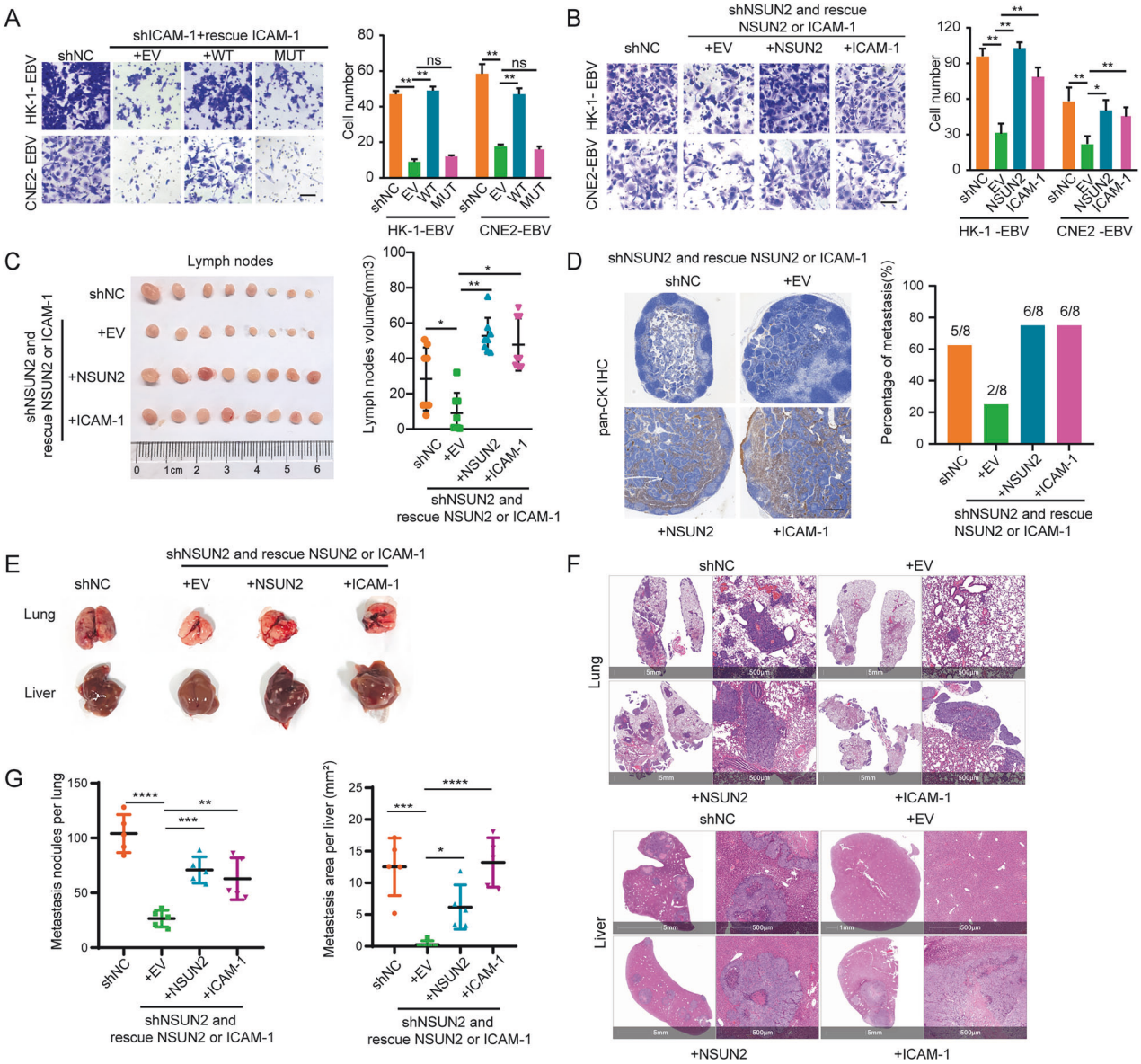

Fig. 6 m^{5}C modification of ICAM-1 mediates NSUN2-induced NPC metastasis. A Transwell assays showing the migration abilities of HK-1-EBV and CNE2-EBV cells with stable ICAM-1 knockdown by shRNA lentivirus and concurrently re-expression of wide-type ICAM-1 (WT) or mutant lacking m^{5}C modification site (MUT). Statistics of three biological replicates are presented on the right. Scale bar, 50μm. **B** Transwell assays showing the migration abilities of HK-1-EBV and CNE2-EBV cells with stable NSUN2 knockdown by shRNA lentivirus and concurrently re-expression of wide-type ICAM-1 or NSUN2. Statistics of three biological replicates are provided on the right. Scale bar, 50μm. **C** Growth of lymph node metastasis from mice ($n = 8$ mice/group) with foot-pad inoculation of CNE2-EBV cells described in B. Extracted lymph nodes were imaged (left) and volumed (right) after one month of inoculation. **D** IHC staining with pan-CK antibodies showing tumor metastasis in lymph nodes displayed in (**C**). The metastasis percentage of the lymph nodes is shown on the right. Scale bar, 500 μm. **E** Representative images of the lung and liver from mice ($n = 5$ mice/group) intravenously injected with CNE2-EBV cells described in (**B**). HE staining (**F**) of lung and liver tissue sections from (**E**), with statistical analysis of metastasis rates presented in (**G**). Statistical analyses were performed using appropriate tests based on data distribution: one-way ANOVA test was used for (**A**, **B**, **C**, **G**). *$P < 0.05$, ** $P < 0.01$, *** $P < 0.001$, **** $P < 0.0001$.

chemotherapy, which, although effective in early-stage disease, remain limited in patients with metastatic disease or recurrent NPC, or in those who are refractory to conventional therapies [54]. Our functional experiments demonstrate that depletion of NSUN2, along with modulation of YBX3 and ICAM-1, significantly inhibits NPC metastasis to lymph node, lung, and liver. These results suggest that targeting this pathway could complement or enhance existing treatment modalities, particularly for advanced disease. Importantly, our clinical analyses show that approximately 30% of NPC patients exhibit concurrent high expression of NSUN2, YBX3, and ICAM-1. This subset of patients tends to present with more advanced disease and poorer prognosis, indicating that therapeutic interventions aimed at disrupting the NSUN2/YBX3/ICAM-1 axis may be especially beneficial in this high-risk group.

In summary, our study establishes a direct functional link connecting EBV infection, RNA m^{5}C modification, and NPC metastasis. We demonstrate that EBV infection elevates LMP1 expression, activating the NF-κB signaling pathway, to promote NSUN2 expression and thus increase RNA m^{5}C modification of ICAM-1 transcripts. These m^{5}C-modified ICAM-1 are specifically recognized by YBX3, a novel RNA m^{5}C reader protein identified here, which subsequently recruits PABPC1 through the cold shock domain to promote efficient ICAM-1 translation (Fig. 7G). These discoveries highlight RNA m^{5}C modification as a critical post-

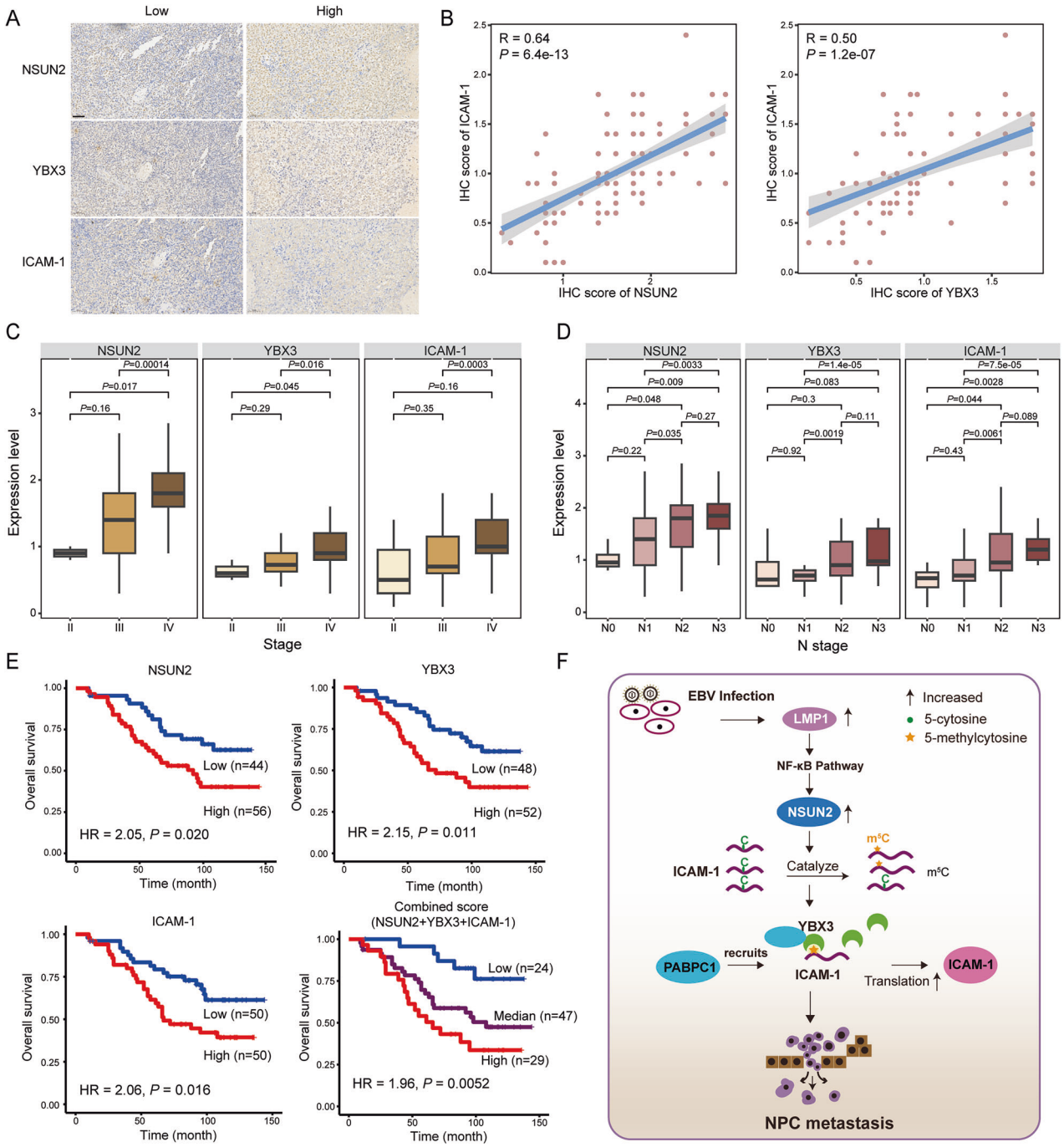

Fig. 7 Clinical relevance of NSUN2, YBX3, and ICAM-1 in NPC patients. A Representative images of IHC staining showing high or low expression of NSUN2, YBX3, and ICAM-1 proteins in tumor tissues from the same NPC patients ($n = 100$). Scale bar, 50μm. **B** Pearson correlation analysis of ICAM-1 with NSUN2 or YBX3 expression based on IHC scores in NPC patients ($n = 100$). Box plots depicting the correlations between the expression levels of NSUN2, YBX3, or ICAM-1 and clinicopathological features such as tumor grade (**C**), N stage (**D**). Expression was based on IHC staining scores in NPC patients ($n = 100$)**. E** Kaplan-Meier survival analysis illustrating patient outcomes based on the individual or combined expression of NSUN2, YBX3, and ICAM-1, using IHC staining scores in NPC patients ($n = 100$). **F** Schematic diagram of a proposed model for EBV-induced m^5C modification in NPC metastasis. EBV encodes LMP1 to upregulate NSUN2 via NF-κB signaling activation, leading to increased m^5C modification of ICAM-1 RNA. The m^5C-modified ICAM-1 is recognized by YBX3, a novel RNA m^5C reader protein, recruiting PABPC1 through its CSD to enhance ICAM-1 translation and thereby promoting tumor metastasis.

transcriptional regulatory mechanism in EBV-associated NPC metastasis and suggest that NSUN2, YBX3, and ICAM-1 represent promising biomarkers and therapeutic targets, pending validation in larger clinical studies. Despite these insights, we acknowledge several limitations to our current study. First, although we focused specifically on RNA m^5C modifications, it remains possible that other RNA modifications also contribute to EBV-induced tumor metastasis, warranting further investigation. Second, our data reveal widespread m^5C modifications upon EBV infection, suggesting additional m^5C-modified transcripts beyond ICAM-1 may also significantly influence NPC pathogenesis, a direction deserving future investigation.

DATA AVAILABILITY

The raw sequence data reported in this paper have been deposited in the Genome Sequence Archive (Genomics, Proteomics & Bioinformatics 2025) in the National Genomics Data Center (Nucleic Acids Res 2025), China National Center of Bioinformation / Beijing Institute of Genomics, Chinese Academy of Sciences (GSA-Human: HRA013888), which are publicly accessible at https://ngdc.cncb.ac.cn/gsa-human. Key raw data are available on the Research Data Deposit (RDD, RDDB2026181374) public platform (http://www.researchdata.org.cn).

REFERENCES

1. Chen YP, Chan ATC, Le QT, Blanchard P, Sun Y, Ma J. Nasopharyngeal carcinoma. Lancet. 2019;394:64–80.
2. Cao SM, Simons MJ, Qian CN. The prevalence and prevention of nasopharyngeal carcinoma in China. Chin J Cancer. 2011;30:114–9.
3. Wong KCW, Hui EP, Lo KW, Lam WKJ, Johnson D, Li L, et al. Nasopharyngeal carcinoma: an evolving paradigm. Nat Rev Clin Oncol. 2021;18:679–95.
4. Yang Y, Qu S, Li J, Hu C, Xu M, Li W, et al. Camrelizumab versus placebo in combination with gemcitabine and cisplatin as first-line treatment for recurrent or metastatic nasopharyngeal carcinoma (CAPTAIN-1st): a multicentre, randomised, double-blind, phase 3 trial. Lancet Oncol. 2021;22:1162–74.
5. Wang Z, LU X, YANG Y, LU Y. Inflammatory granuloma of the trachea: a rare case with Epstein-Barr virus infection. J Zhejiang Univ Sci B. 2023;24:539–42.
6. Kamran SC, Riaz N, Lee N. Nasopharyngeal carcinoma. Surg Oncol Clin N Am. 2015;24:547–61.
7. Chen YS, Yang WL, Zhao YL, Yang YG. Dynamic transcriptomic m5C and its regulatory role in RNA processing. Wiley Interdiscip Rev RNA. 2021;12:e1639.
8. Edelheit S, Schwartz S, Mumbach MR, Wurtzel O, Sorek R. Transcriptome-wide mapping of 5-methylcytidine RNA. PLoS Genet. 2013;9:e1003602–e16.
9. Ito S, Shen L, Dai Q, Wu SC, Collins LB, Swenberg JA, et al. Tet proteins can convert 5-methylcytosine to 5-formylcytosine and 5-carboxylcytosine. Science. 2011;333:1300–5.
10. Yang X, Yang Y, Sun BF, Chen YS, Xu JW, Lai WY, et al. 5-methylcytosine promotes mRNA export - NSUN2 as the methyltransferase and ALYREF as an m^5C reader. Cell Res. 2017;27:606–25.
11. Wang Y, Wei J, Feng L, Li O, Huang L, Zhou S, et al. Aberrant m5C hypermethylation mediates intrinsic resistance to gefitinib through the NSUN2/YBX1/QSOX1 axis in EGFR-mutant non-small-cell lung cancer. Mol Cancer. 2023;22:81.
12. Hu Y, Chen C, Tong X, Chen S, Hu X, Pan B, et al. NSUN2 modified by SUMO-2/3 promotes gastric cancer progression and regulates mRNA m5C methylation. Cell Death Dis. 2021;12:842.
13. Wang N, Chen RX, Deng MH, Wei WS, Zhou ZH, Ning K, et al. m(5)C-dependent cross-regulation between nuclear reader ALYREF and writer NSUN2 promotes urothelial bladder cancer malignancy through facilitating RABL6/TK1 mRNAs splicing and stabilization. Cell Death Dis. 2023;14:139.
14. Jin Y, Yao J, Fu J, Huang Q, Luo Y, You Y, et al. ALYREF promotes the metastasis of nasopharyngeal carcinoma by increasing the stability of NOTCH1 mRNA. Cell Death Dis. 2024;15:578.
15. Lang F, Singh RK, Pei Y, Zhang S, Sun K, Robertson ES. EBV epitranscriptome reprogramming by METTL14 is critical for viral-associated tumorigenesis. PLoS Pathog. 2019;15:e1007796.
16. Xia TL, Li X, Wang X, Zhu YJ, Zhang H, Cheng W, et al. N(6)-methyladenosine-binding protein YTHDF1 suppresses EBV replication and promotes EBV RNA decay. EMBO Rep. 2021;22:e50128.
17. Zhang P, He Q, Lei Y, Li Y, Wen X, Hong M, et al. m(6)A-mediated ZNF750 repression facilitates nasopharyngeal carcinoma progression. Cell Death Dis. 2018;9:1169–80.
18. Xu YY, Li T, Shen A, Bao XQ, Lin JF, Guo LZ, et al. FTO up-regulation induced by MYC suppresses tumour progression in Epstein-Barr virus-associated gastric cancer. Clin Transl Med. 2023;13:e1505.
19. Henry BA, Kanarek JP, Kotter A, Helm M, Lee N. 5-methylcytosine modification of an Epstein-Barr virus noncoding RNA decreases its stability. RNA. 2020;26:1038–48.
20. Liu Y, He S, Wang XL, Peng W, Chen QY, Chi DM, et al. Tumour heterogeneity and intercellular networks of nasopharyngeal carcinoma at single cell resolution. Nat Commun. 2021;12:741.
21. Zhang L, MacIsaac KD, Zhou T, Huang P-Y, Xin C, Dobson JR, et al. Genomic analysis of nasopharyngeal carcinoma reveals TME-based subtypes. genomic subtypes of nasopharyngeal carcinoma. 2017;15:1722–32.
22. García Vílcheza R, Sevillab A, Blanco S. Post-transcriptional regulation by cytosine-5 methylation of RNA. Biochim Biophys Acta Gene Regul Mech. 2019;1862:240–52.
23. Liu Y, He S, Wang XL, Peng W, Chen QY, Chi DM, et al. Tumour heterogeneity and intercellular networks of nasopharyngeal carcinoma at single cell resolution. Nat Commun. 2021;12:741–58.
24. Chen X, Li A, Sun BF, Yang Y, Han YN, Yuan X, et al. 5-methylcytosine promotes pathogenesis of bladder cancer through stabilizing mRNAs. Nat Cell Biol. 2019;21:978–90.
25. Wang X, Wang M, Dai X, Han X, Zhou Y, Lai W, et al. RNA 5-methylcytosine regulates YBX2-dependent liquid-liquid phase separation. Fundam Res. 2022;2:48–55.
26. Wang Y, Wei J, Feng L, Li O, Huang L, Zhou S, et al. Aberrant m5C hypermethylation mediates intrinsic resistance to gefitinib through NSUN2 YBX1 QSOX1 axis in EGFR-mutant non-small-cell lung cancer. Mol Cancer. 2023;22:81–99.
27. Ma HL, Bizet M, Soares Da Costa C, Murisier F, de Bony EJ, Wang M-K, et al. SRSF2 plays an unexpected role as a reader of m5C on mRNA, linking epitranscriptomics to cancer. Mol Cell. 2023;83:4239–54.
28. Yang Y, Wang L, Xiao H, WenLan Y, Mengmeng Z, HaiLi M, et al. RNA 5-methylcytosine facilitates the maternal-to-zygotic transition by preventing maternal mRNA decay. Mol Cell. 2019;75:1188–202.
29. Gao J, Tang YD, Hu W, Zheng C. When poly(A) binding proteins meet viral infections. J Virol. 2022;96:e0013622.
30. Grosset Christophe, Chen C-YA, Xu N, Sonenberg N, Jacquemin-Sablon H, Shyu A-B. A mechanism for translationally coupled mRNA turnover interaction between the Poly(A) tail and a c-fos RNA coding determinant via a protein complex. Cell. 2000;103:29–40.
31. Xie J, Kozlov G, Gehring K. The "tale" of poly(A) binding protein: the MLLE domain and PAM2-containing proteins. Biochim Biophys Acta. 2014;1839:1062–8.
32. Pang PS, Liu T, Lin W, Tsang CM, Yip YL, Zhou Y, et al. Defining early events of Epstein-Barr virus (EBV) infection in immortalized nasopharyngeal epithelial cells using cell-free EBV infection. J Gen Virol. 2019;100:999–1012.
33. Scott RS. Epstein-Barr virus: a master epigenetic manipulator. Curr Opin Virol. 2017;26:74–80.
34. Cai L, Ye Y, Jiang Q, Chen Y, Lyu X, Li J, et al. Epstein–Barr virus-encoded microRNA BART1 induces tumour metastasis by regulating PTEN-dependent pathways in nasopharyngeal carcinoma. Nat Commun. 2015;6:1–13.
35. Zou S, Huang Y, Yang Z, Zhang J, Meng M, Zhang Y, et al. NSUN2 promotes colorectal cancer progression by enhancing SKIL mRNA stabilization. Clin Transl Med. 2024;14:e1621.
36. Chen B, Deng Y, Hong Y, Fan L, Zhai X, Hu H, et al. Metabolic recoding of NSUN2-mediated m(5)C modification promotes the progression of colorectal cancer via the NSUN2/YBX1/m(5)C-ENO1 positive feedback loop. Adv Sci. 2024;11:e2309840.
37. Chen T, Xu ZG, Luo J, Manne RK, Wang Z, Hsu CC, et al. NSUN2 is a glucose sensor suppressing cGAS/STING to maintain tumorigenesis and immunotherapy resistance. Cell Metab. 2023;35:1782–1798.e8.
38. Zhang W, Guo Q, Liu G, Zheng F, Chen J, Huang D, et al. NKILA represses nasopharyngeal carcinoma carcinogenesis and metastasis by NF-kappaB pathway inhibition. PLoS Genet. 2019;15:e1008325.
39. Zheng Z, Qu JQ, Yi HM, Ye X, Huang W, Xiao T, et al. MiR-125b regulates proliferation and apoptosis of nasopharyngeal carcinoma by targeting A20/NF-kappaB signaling pathway. Cell Death Dis. 2017;8:e2855.
40. Wang Y, Wang Y, Patel H, Chen J, Wang J, Chen ZS, et al. Epigenetic modification of m(6)A regulator proteins in cancer. Mol Cancer. 2023;22:102.
41. Matsumoto K, Wolffe AP. Gene regulation by Y-box proteins: coupling control of transcription and translation. Trends Cell Biol. 1998;8:318–23.
42. Sun Y, Li Z, Wang W, Zhang X, Li W, Du G, et al. Identification and verification of YBX3 and its regulatory gene HEIH as an oncogenic system: a multidimensional analysis in colon cancer. Front Immunol. 2022;18:957865–83.
43. Xiang Y, Zhou S, Hao J, Zhong C, Ma Q, Sun Z, et al. Development and validation of a prognostic model for kidney renal clear cell carcinoma based on RNA-binding protein expression. Aging. 2020;12:25356–72.
44. Sears D, Luong P, Yuan M, Nteliopoulos G, Man Y, Melo J, et al. Functional phosphoproteomic analysis reveals cold-shock domain protein A to be a Bcr-Abl effector-regulating proliferation and transformation in chronic myeloid leukemia. Cell Death Dis. 2010;4:e93.
45. Yasen M, Obulhasim G, Kajino K, Mogushi K, Mizushima H, Tanaka S, et al. DNA-binding protein A expression and methylation status in hepatocellular carcinoma and the adjacent tissue. Int J Oncol. 2012;40:789–97.
46. Fan X, Xie X, Yang M, Wang Y, Wu H, Deng T, et al. YBX3 mediates the metastasis of nasopharyngeal carcinoma via PI3K/AKT signaling. Front Oncol. 2021;17:617621–32.
47. Kong R, Wei W, Man Q, Chen L, Jia Y, Zhang H, et al. Hypoxia-induced circ-CDYL-EEF1A2 transcriptional complex drives lung metastasis of cancer stem cells from hepatocellular carcinoma. Cancer Lett. 2023;578:216442.
48. Péneau C, Imbeaud S, La Bella T, Hirsch TZ, Caruso S, Calderaro J, et al. Hepatitis B virus integrations promote local and distant oncogenic driver alterations in hepatocellular carcinoma. Gut. 2022;71:616–26.
49. Engels R, Falk L, Albanese M, Keppler OT, Sewald X. LFA1 and ICAM1 are critical for fusion and spread of murine leukemia virus in vivo. Cell Rep. 2022;38:110279.

50. Taftaf R, Liu X, Singh S, Jia Y, Dashzeveg NK, Hoffmann AD, et al. ICAM1 initiates CTC cluster formation and trans-endothelial migration in lung metastasis of breast cancer. Nat Commun. 2021;12:4867.
51. Holland M, Castro FV, Alexander S, Smith D, Liu J, Walker M, et al. RAC2, AEP, and ICAM1 expression are associated with CNS disease in a mouse model of pre-B childhood acute lymphoblastic leukemia. Blood. 2011;118:638–49.
52. Kang MS, Kieff E. Epstein–Barr virus latent genes. Exp Mol Med. 2015;47:e131.
53. Masy E, Adriaenssens E, Montpellier C, Crepieux P, Mougel A, Quatannens B, et al. Human monocytic cell lines transformed in vitro by Epstein-Barr virus display a type II latency and LMP-1-dependent proliferation. J Virol. 2002;76:6460–72.
54. Jiang W, Lv JW, Tang LL, Sun Y, Chen YP, Ma J. Enhancing efficacy and reducing toxicity: Therapeutic optimization in locoregionally advanced nasopharyngeal carcinoma. Cell Rep Med. 2024;5:101594.

ACKNOWLEDGEMENTS

We thank all the participants in the study, and staff at the biobank of SYSUCC for processing sample preparation and staff at the High-Throughput Analysis Platform (HTAP) of SYSUCC for data generation and processing.

AUTHOR CONTRIBUTIONS

J-XB, and C-LL conceived this study; J-XB, C-LL and X-ZW designed the experiments and wrote the manuscript; X-ZW, and J-XJ carried out the experiments; Y-QL, Y-L, and W-L performed bioinformatics analyses; S-YY and D-MC assisted with mice experiment. P-PW and H-QH engaged in data acquisition. All authors have read and approved the final manuscript.

FUNDING

This work was supported by the National Natural Science Foundation (82130078, 82261160657, and 82192894), Fundamental and Interdisciplinary Disciplines Breakthrough Plan of the Ministry of Education of China (JYB2025XDXM608), the Guangdong Basic and Applied Basic Research Foundation (2024A1515013061), the China Postdoctoral Science Foundation (2023M744053), Chang Jiang Scholars Program (J-XB), Cancer Innovative Research Program of Sun Yat-sen University Cancer Center (CIRP-SYSUCC-0020), Young Talents Program of Sun Yat-sen University Cancer (Center YTP-SYSUCC-0075) and Hong Kong Research Grant Council (RGC) Theme-based Research Scheme Funds (T12-703/22-R and T12-703/23-N).

COMPETING INTERESTS

The authors declare no competing interests.

ETHICS DECLARATIONS

The collection and use of all clinical samples were approved by the Ethics Committee of SYSUCC, and written informed consent was obtained from all patients prior to specimen collection. All animal experiments were conducted in accordance with the guidelines and ethical regulations approved by the Institutional Animal Care and Use Committee at SYSUCC.

ADDITIONAL INFORMATION

Supplementary information The online version contains supplementary material available at https://doi.org/10.1038/s41418-026-01719-4.

Correspondence and requests for materials should be addressed to Jin-Xin Bei or Chun-Ling Luo.

Reprints and permission information is available at http://www.nature.com/reprints

Publisher's note Springer Nature remains neutral with regard to jurisdictional claims in published maps and institutional affiliations.

Open Access This article is licensed under a Creative Commons Attribution 4.0 International License, which permits use, sharing, adaptation, distribution and reproduction in any medium or format, as long as you give appropriate credit to the original author(s) and the source, provide a link to the Creative Commons licence, and indicate if changes were made. The images or other third party material in this article are included in the article's Creative Commons licence, unless indicated otherwise in a credit line to the material. If material is not included in the article's Creative Commons licence and your intended use is not permitted by statutory regulation or exceeds the permitted use, you will need to obtain permission directly from the copyright holder. To view a copy of this licence, visit http://creativecommons.org/licenses/by/4.0/.

© The Author(s) 2026